

STUDY OF THERMAL DISTRIBUTION AND CLADDING GEOMETRY DURING LASER METAL DEPOSITION PROCESS USING FINITE ELEMENT ANALYSIS

Andrei Rusu [1,4], Alexandru Bunea[2,4] and Daniel Ghiculescu[3]
[1] Faculty of Industrial Engineering and Robotics, Polytechnic University of Bucharest, andrei.rusu@inflpr.ro
[2] Faculty of Industrial Engineering and Robotics, Polytechnic University of Bucharest, alexandru.bunea@inflpr.ro
[3] Faculty of Industrial Engineering and Robotics, Polytechnic University of Bucharest, daniel.ghiculescu@upb.ro
[4]Center for Advanced Laser Technologies, National Institute for Laser, Plasma and Radiation Physics (INFLPR), Ilfov, 077125 Magurele, Romania

ABSTRACT: The paper deals with additive manufacturing process for coating and 3D printing metallic materials known in literature as laser cladding, laser melting deposition, laser engineering net shaping or direct energy deposition. In this process a melt pool was generated at the interaction of the laser beam with the blown powder guided through a copper nozzle. A 3D finite element model was established to simulate laser cladding process taking into account heat transfer in solids and geometry deformation modules from COMSOL Multiphysics software. A time-dependent study was conducted to manage the computational time of the numerical model. Boundary conditions were established by introducing a Gaussian distribution for the laser energy, as well as for the velocity and shape of the resulting track. Additionally, the thermal properties of the material under investigation were taken into account. Thermal analysis was conducted to determine the temperature history during the process using a heat transfer module, while the dynamic shape of the molten zone was represented by a moving mesh based on a deformed geometry module.
KEYWORDS: additive manufacturing, laser cladding, melt pool, heat transfer, cladding height, finite element.

1. INTRODUCTION

Additive manufacturing is a laser processing technique for coating or 3D printing metallic or ceramics materials, also known in the literature as Laser Cladding (LC), Laser Melting Deposition (LMD), Laser Engineering Net Shaping (LENS) or Direct Energy Deposition (DED) [1], [2], [3], [4]. This technique allows the manufacture of bulkmaterials from Computer Aided Design (CAD) drawings by a succession of superposed deposited layers comprising laser melting–solidification effects of powder stream. More precisely, during LMD processing, the laser tracks generate a molten pool on a metallic substrate. The metal/ceramic powder stream is directed into the laser-induced melt pool to create a new layer and by repeating this procedure in a layer-by-layer manner a 3D part with complex geometry is fabricated [5]. Another important application of this technique includes refurnishing–repairing of damaged parts [6]. During the LMD, the deposited material experience different thermal variations due to the fast heating-cooling phenomena, which influence the microstructure. Thus, these effects significantly impact the material's mechanical properties.

Opaqueness and the rapid process of melting and solidification of the melt pool are the main reasons why real time detection and observation during the laser processing is challenging. [7]. Rapid expansion of computer know-how, numerical and analytical simulation has become consistent methods used to forecasting and examining the progression of solidification process [8].

Literature presents numerous studies about mathematical and physical thermal models for single track laser cladding processes [9], [10], [11]. F. Caiazzo et al. [12] created a finite element analysis and simulation for the laser cladding of aluminum, focusing on both geometry of the cladding and the thermal distribution in the material. Processing parameters and their outcomes are studied in F. Wirth et al. [13]. Characteristics like isotropic and temperature dependent were taken into account while creating the simulation of temperature and velocity of the melt pool. Wei Ya et al. [14] created a numerical model capable of predicting the heat affected zone and depth of the melt pool by assigning process parameters for laser cladding in COMSOL Multiphysics. In the article of B. K. Panda et al [15], was suggested a numerical model that can predict the interface between substrate and cladding layer utilizing a set of parameters and a function which is time dependent. B. K. Panda et al [15] completed the article with an experiment that matches the numerical simulation results.

The objective of this paper is to achieve a numerical model that can predict the cladding geometry and thermal distribution. This 3D thermal model of laser cladding consider the parameters and the effects of powder utilization rate and powder stream density. Using functions that take into account process parameters like: laser power, cladding speed, powder feed rate and powder utilization rate we calculate the geometry of single-track cladding. Finite element simulation software like COMSOL MULTIPHYSICS® v5.5 (100 District Avenue, Burlington, USA) can solve the equations for conservation of energy and mass. Moving mesh is used to describe the geometry of the cladding, which considers mass addition, melting and material thermal properties. For the computation were taken into account physical and thermal properties, for the solid phase of both materials for coating and substrate.

2. MATERIALS AND METHODS

Laser Melting Deposition (LMD), commonly referred to as Laser Cladding, is an additive manufacturing process that offers several advantages in industrial applications, including repair, coating, and 3D printing. This process involves feeding one or more powder materials through a nozzle using a mixture of argon to prevent oxidation and helium for particle transportation. The powders are delivered in a specific weight percentage ratio in order to achieve an optimal material deposition. Figure 1 illustrates this process.

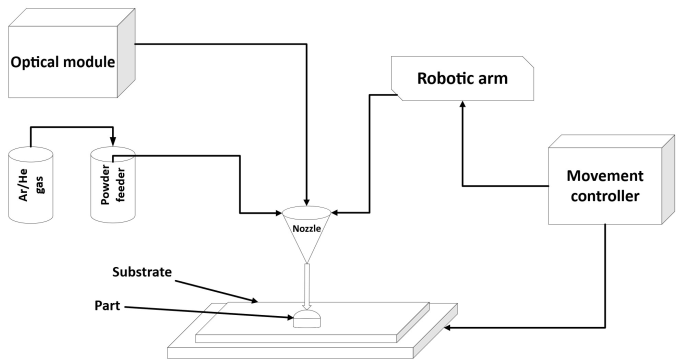

Figure 1. Schematic diagram of LMD technology

When the powder is blown into the laser beam on substrate the melting pool takes place. Dissipation of the temperature in materials plays a crucial role in the solidification behavior and influences the final form of the melt pool. The schematics of the process principle can be observed in figure 2.

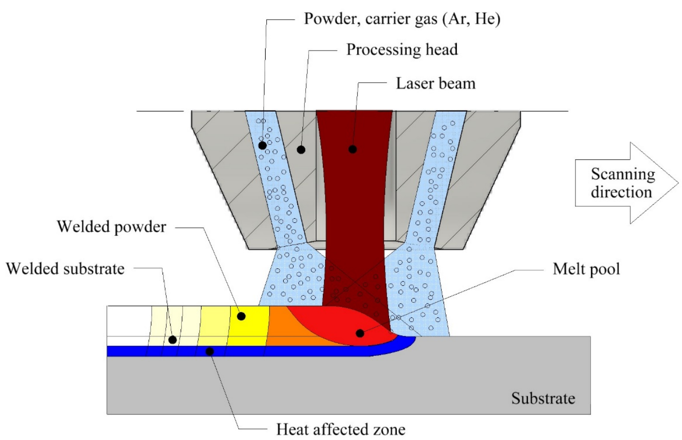

Figure 2. LMD process principle

We attempt to create a numerical model that could be applied on specific cases for simulating formation mechanism of laser cladding.

In order to achieve this goal, COMSOL Multiphysics 5.5 was utilized with the Heat Transfer and Deformed Geometry modules, combined with a Time-Dependent study to create this finite element analysis.

To improve numerical model time calculations and software resources consumption the following simplifications were made [16]:

1. Substrate and cladding powder have the following characteristics: continuous, isotropic and temperature dependent.

2. Melt pool effects like fluid flow and material evaporation are ignored.

3. The temperature of the powder before contact with melt pool is negligible

To finalize the finite element analysis, the stages outlined in figure 3 must be followed.

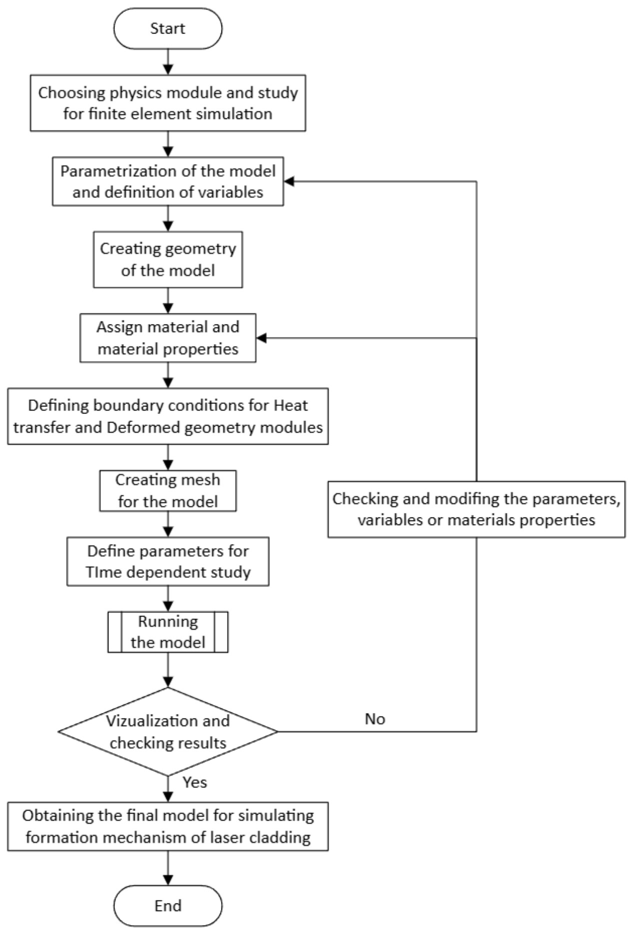

Figure 3. Schematic diagram of COMSOL Multiphysics simulation model

2.1 Parametrization of the model

The parameters and variables used to define thermal characteristics, the laser heat source and the form of the formed track are essential for creating the model geometry, as exemplified in figure 4.

Name	Expression	Value	Description
A1	0.2	0.2	Absortivity
D	3 [mm]	0.003 m	Beam diameter
emi	0.9	0.9	Emissivity
h1	20[W/(m^2*K)]	20 W/(m²·K)	Heat transfer coefficient
speed	8.68 [mm/s]	0.00868 m/s	Laser scan speed
H1	6 [mm]	0.006 m	Height big parallelepipeds
W1	8 [mm]	0.008 m	Width big parallelepipeds
L1	50 [mm]	0.05 m	Lenght big parallelepipeds
h_small	2 [mm]	0.002 m	Height small parallelepipeds
w_small	10 [mm]	0.01 m	Width small parallelepipeds
l_small	50 [mm]	0.05 m	Lenght small parallelepipeds
Ta	293.15 [K]	293.15 K	Ambient temperature
P	931 [W]	931 W	Laser power
sigma	D/6	5E-4 m	Gauss distribution on the spot
x0	0 [mm]	0 m	Initial position/Reference point
TtopIn718	1350+273.15 [K]	1623.2 K	Melting point of In718
y0	50 [mm]	0.05 m	Initial position/Reference point
tstop	(L1)/speed	5.7604 s	Processing time
n	0.7	0.7	Powder utilization rate
m	19.15 [g/min]	3.1917E-4 kg/s	Powder feed rate
rho_In718	8.19 [g/cm^3]	8190 kg/m³	Density of In718

a) Parameters used for creating numerical model

Name	Expression	Unit	Description
Ed	P/(pi*0.05*D^2)	W/m²	Ennergy density
G_space	exp(-((x-xr)^2/(2*sigma^2)+(y-yr)^2/(2*sigma^2)))		Gaussian space
Pg	A1*Ed*G_space	W/m²	Laser heat source
xr	x0	m	Current position x
yr	y0-speed*t	m	Current position y
comp1	(n*m)/(rho_In718*pi*(D/2)^2)	m/s	Mesh speed
comp2	exp(-((x-xr)^2/(2*(D/2)^2)+(y-yr)^2/(2*(D/2)^2)))		Component 2 of mesh speed
Mesh_speed	comp1*comp2	m/s	Shape of the formed track

b) Variables used for positioning and physics modules

Figure 4. Parameters and variables used in model

The Gaussian heat source model, equation (1), was developed in a previous work [17]. Where A1 is absorptivity; P designates laser power; D designates beam diameter; x, y, xr and yr are the initial and current coordinates of laser and sigma is the Gauss distribution in the spot.

$$Pg = \frac{A1*P}{\pi*0.05*D^2} * \sqrt{-\frac{(x-xr)^2+(y-yr)^2}{2*sigma^2}} \quad (1)$$

Equation (2) is used for calculation the velocity and shape of formed track [18]. Where n is powder utilization rate; m is powder feed ratio; rho_In718 is density of In718; D is beam diameter; and x, y, xr and yr are the initial and current coordinates of the boundary.

$$Mesh\_speed = \frac{n*m}{rho\_In718*\pi*\left(\frac{D}{2}\right)^2} * \sqrt{-\frac{(x-xr)^2+(y-yr)^2}{2*\left(\frac{D}{2}\right)^2}} \quad (2)$$

Material and its properties were allocated from COMSOL library as it is exemplified in figure 5. Inconel 718 (In718) is the chosen material for our numerical simulation.

Property	Variable	Expression	Unit
Thermal conductivity	k_iso ; kii = k_iso, k...	40[W/(m*K)]	W/(m·K)
Resistivity	res_iso ; resii = res_...	0.00000132[ohm*m]	Ω·m
Coefficient of thermal expansion	alpha_iso ; alphaii...	12.2*10^(-6)[1/K]	1/K
Heat capacity at constant pressure	Cp	435[J/(kg*K)]	J/(kg·K)
Electrical conductivity	sigma_iso ; sigmaii...	0.8[MS/m]	S/m
Density	rho	rho_In718	kg/m³

Figure 5. Material properties allocation of Inconel 718

3. RESULTS AND DISCUSSIONS

3.1 Geometry of the model

The 3D geometry (figure 6) was created using Comsol Multiphysics 5.5 built-in functions. With the help of the geometric parameters previously mentioned, two substrates with different dimensions were built (H1, W1, L1), respectively (h_small, w_small, l_small) with the purpose to run different types of meshing.

The boolean operations "difference" and "union" were used consecutively to create a final form of geometry that checks all the requirements of the study.

This geometry is influenced by all the physics and study modules that were added at the beginning of the numerical simulation.

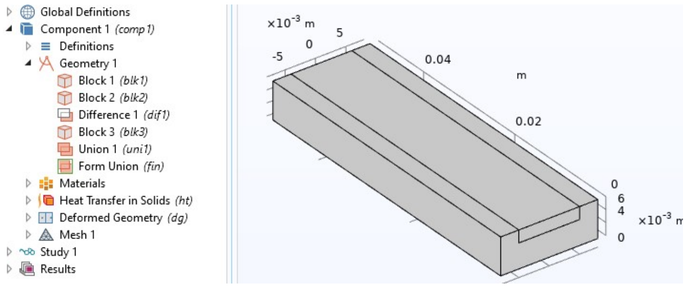

Figure 6. The 3D geometry model

3.2 Physics modules and boundary conditions

For the heat transfer in solids module, we have the following conditions:

-Initial Values, Thermal Insulation, Heat Flux 1, Heat Flux 2, Surface-to-Ambient Radiation 1.

Initial values (figure 7) represent ambient temperature which was set at 20 ˚C or 293,15 K and signify a thermal parameter at the beginning of modulation.

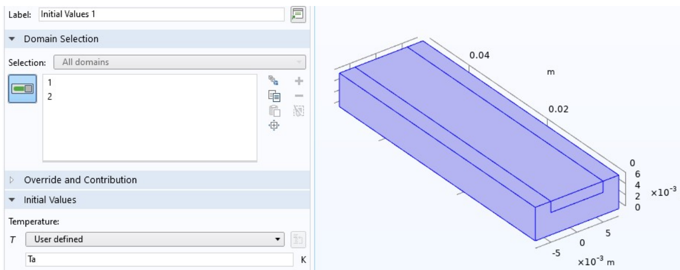

Figure 7. Initial values

Initially, on the thermal insulation condition, all the surfaces of the model are insulated.

After adding the requirements of the next conditions all the preliminary surfaces that were thermal insulated will be overridden as can be seen in figure 8.

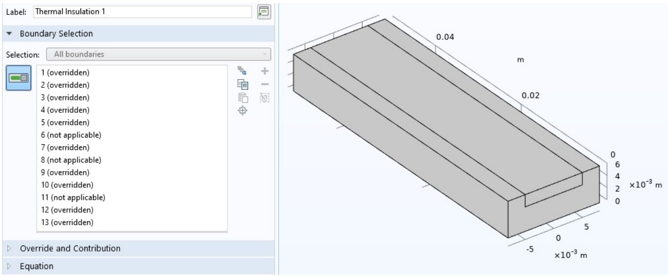

Figure 8. Thermal insulation

To boundary condition, Heat Flux 1 (figure 9) was allocated as heat source, defined earlier as variable “Pg”. Thermic heat source consists of Gaussian power distribution on the laser spot.

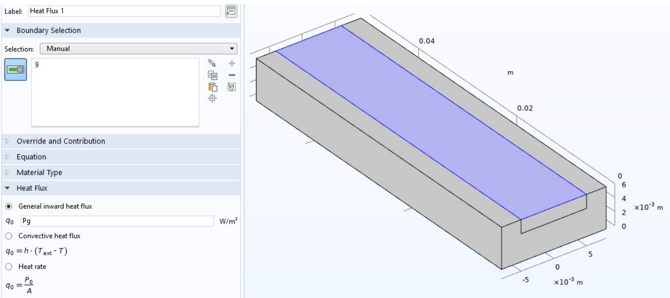

Figure 9. Heat Flux 1 – Heat source

Boundary condition, Heat Flux 2, was used for cooling the part at room temperature using heat transfer coefficient defined as parameter “h1” in figure 10.

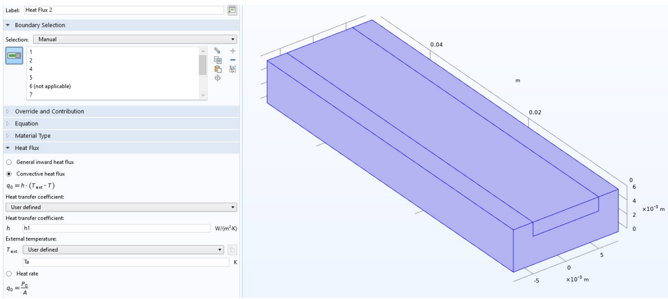

Figure 10. Heat Flux 2 – Cooling at room temperature

Surface-to-Ambient Radiation 1 was the boundary condition which describes radiation of surface to the ambiental environment through emissivity coefficient defined as “emi” in figure 11.

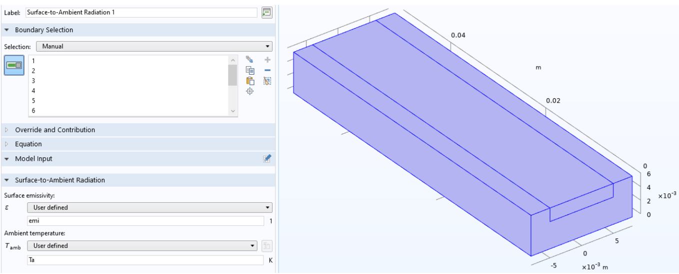

Figure 11. Surface-to-Ambient Radiation

The Deformed Geometry module has the following conditions: Prescribe Mesh Displacement 1, Free Deformation 1 and Prescribed Mesh Velocity 1.

Prescribe Mesh Displacement 1 (figure 12) is a condition that comes predefined when adding the deformed geometry module. The default settings of this condition provide a fixed boundary (zero displacement in all direction). After adding the next conditions, the initial surfaces will be overridden or the effect of zero displacement will not be applicable.

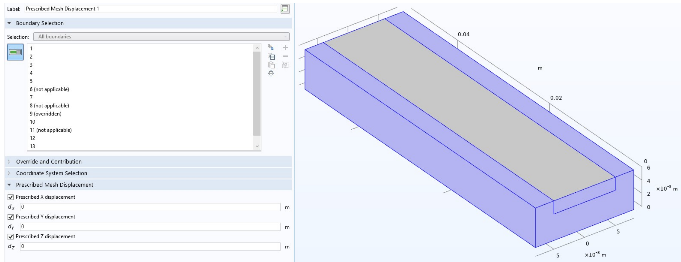

Figure 12. Prescribed Mesh Displacement 1

Condition, Free Deformation 1, was used to give initial values for mesh displacement fields. This condition is useful for constraining the surrounding boundaries and it was combined with the next condition Prescribe Mesh Velocity 1 (figure 13).

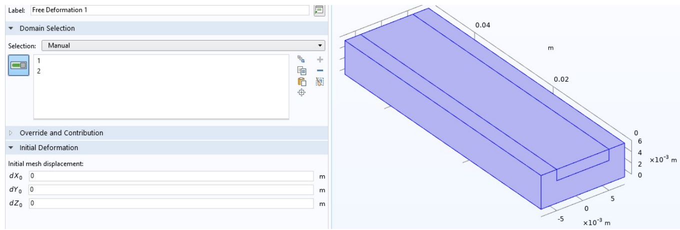

Figure 13. Free deformation 1

Prescribe Mesh Velocity 1 node was used for domains with free displacement. The material from the selected domain proximity moves in accordance with the velocity (figure 14).

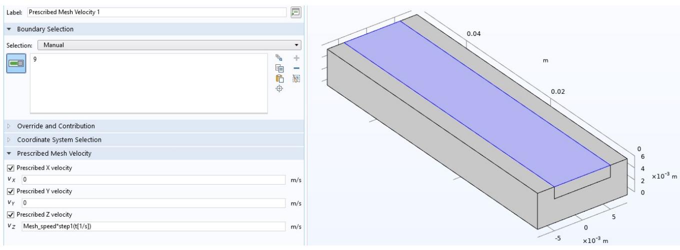

Figure 14. Prescribe Mesh Velocity 1

The function Step 1 was utilized for smoothing the model solver by avoiding numerically unfavorable sharp steps. Using smoothing function on the deformed geometry module can lead to shorted computing time with smooth result and less errors (figure 15).

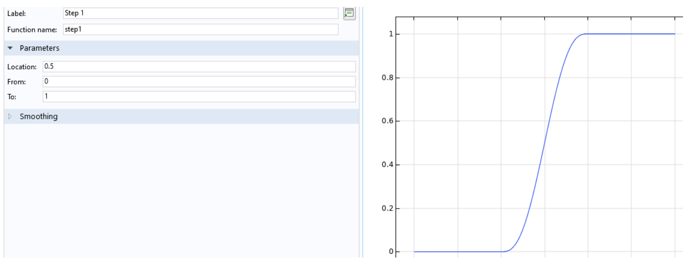

Figure 15. Step 1 function

3.3 Discretization of the model

The mesh generated in Comsol Multiphysics was set to have a tetrahedral form (figure 16). The intersection between any two or more elements in the mesh is defined by sub-elements, like mesh faces, edges or vertex, which are represented in figure 17. The mesh for the interest zone, have extremely fine element for a better result precision. The rest of the part is composed of extremely coarse mesh for a faster program compilation.

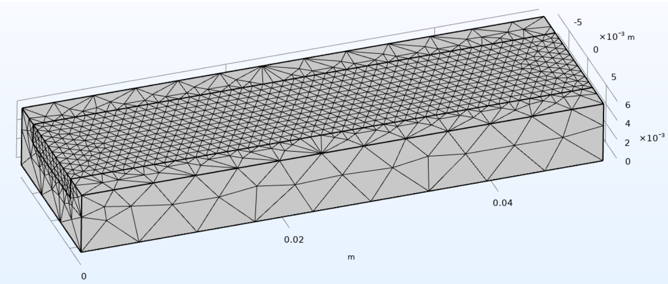

Figure 16. Mesh representation

The overall count of tetrahedral elements included in the two geometries was 21849 with a mean element quality of 0.6352 as shown in figure 17.

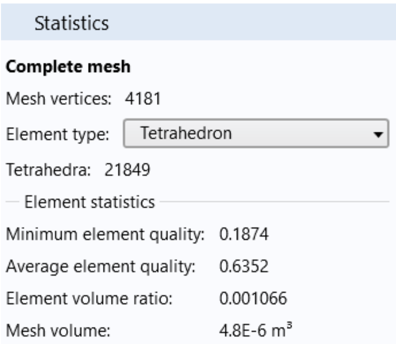

Figure 17. Elements number and quality

3.4 Time dependent parameters

The time-dependent study configuration (Figure 18) was used to create a graphical representation of the LMD process. Utilizing the animation function available in Comsol, we were able to display the material deposited on the substrate with a precision of 0.1 s until the simulation reached the end of the geometry. This representation also included temperature variation, which influenced all the physics modules in this study.

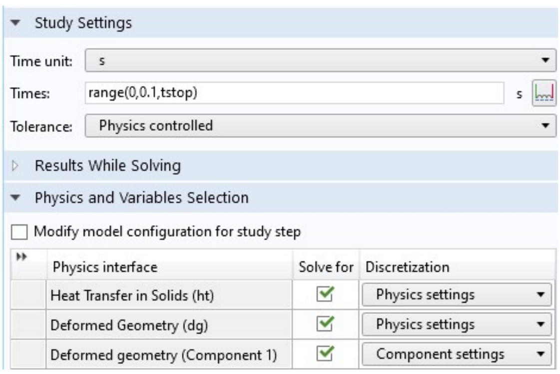

Figure 18. Time dependent configuration

3.5 Results

The influence of different parameters on the temperature filed and cladding height were studied by COMSOL. The model accounts a single-track cladding layer in the direction of scanning speed. The temperature field distribution and cladding height were analyzed throughout the entire runtime of the computation time with an increment of 0.1 s, from 0 s to the 5.7 s.

The temperature of the part during the process varied between 291.9 K and 2695.1 K. Minimum temperature of the part was calculated as the coldest point during process and maximum temperature was considered as the hottest point during processing time. All the values obtained from COMSOL Multiphysics in terms of temperature are presented in figure 19.

Time (s)	Temperature [K]		Time (s)	Temperature [K]	
	Min	Max		Min	Max
0	291.9	298.6	2.9	293.1	2503.6
0.1	292.6	1869.3	3	293.1	2482.8
0.2	292.8	2067.1	3.1	293.1	2503.7
0.3	293	1989.1	3.2	293.1	2477
0.4	293.1	2071	3.3	293.1	2497.8
0.5	293	2111.2	3.4	293.1	2516.7
0.6	293	2230.1	3.5	293.1	2478.9
0.7	293	2390.1	3.6	293.1	2567.2
0.8	293.1	2421.3	3.7	293.1	2607.8
0.9	293.1	2357.7	3.8	293.1	2518.2
1	293.1	2428.2	3.9	293.1	2487.4
1.1	293.1	2449.1	4	293.1	2483.3
1.2	293.1	2471.5	4.1	293.1	2467.2
1.3	293.1	2549.6	4.2	293.1	2456.7
1.4	293.1	2501.6	4.3	293.1	2461
1.5	293.1	2437.6	4.4	293.1	2558.9
1.6	293.1	2411.6	4.5	293.1	2560.9
1.7	293.1	2407	4.6	293.1	2446.1
1.8	293.1	2457.1	4.7	293.2	2432.6
1.9	293.1	2506	4.8	293.3	2484.3
2	293.1	2449.1	4.9	293.4	2465.8
2.1	293.1	2539.6	5	293.7	2498.8
2.2	293.1	2476.2	5.1	293.4	2545.2
2.3	293.1	2461.4	5.2	294.7	2504
2.4	293.1	2473.5	5.3	295.8	2483.6
2.5	293.1	2463.7	5.4	297.3	2573.8
2.6	293.1	2447	5.5	299.5	2463.8
2.7	293.1	2483.2	5.6	302.5	2551.5
2.8	293.1	2525.8	5.7	306.2	2695.1

Figure 19. Values of temperature during processing time

Observing the chart from figure 20 we draw the following conclusions about minimum and maximum temperature. Minimum temperature stays at the same point during processing time, except at the end of the process, because of the slow movement of the laser head the temperature tends to increase. Maximum temperature rises very fast in the first seconds of the program and then has a tendency to remain constant at about 2500 K until the end of the computational time. Variation of the values at the maximum temperature can be influenced by the discretization of the part.

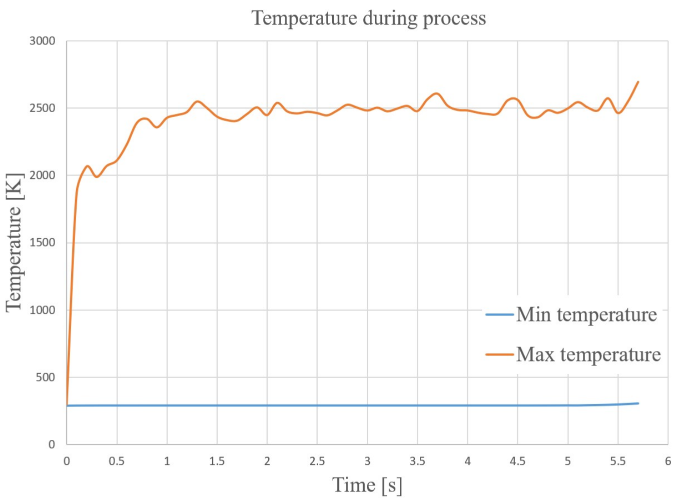

Figure 20. Chart of min and max temperatures

Cladding height (h cladding) was calculated as difference between total height after running the program (h final) and height of the part (h part), which are presented in figure 21.

Time [s]	h part [mm]	h final [m]	h final [mm]	h cladding [mm]	Time [s]	h part [mm]	h final [m]	h final [mm]	h cladding [mm]
0	6	0.00600	6.00	0.00	2.9	6	0.00767	7.67	1.67
0.1	6	0.00600	6.00	0.00	3	6	0.00767	7.67	1.67
0.2	6	0.00601	6.01	0.01	3.1	6	0.00766	7.66	1.66
0.3	6	0.00605	6.05	0.05	3.2	6	0.00766	7.66	1.66
0.4	6	0.00613	6.13	0.13	3.3	6	0.00767	7.67	1.67
0.5	6	0.00627	6.27	0.27	3.4	6	0.00766	7.66	1.66
0.6	6	0.00644	6.44	0.44	3.5	6	0.00767	7.67	1.67
0.7	6	0.00665	6.65	0.65	3.6	6	0.00767	7.67	1.67
0.8	6	0.00687	6.87	0.87	3.7	6	0.00767	7.67	1.67
0.9	6	0.00708	7.08	1.08	3.8	6	0.00766	7.66	1.66
1	6	0.00725	7.25	1.25	3.9	6	0.00767	7.67	1.67
1.1	6	0.00739	7.39	1.39	4	6	0.00767	7.67	1.67
1.2	6	0.00748	7.48	1.48	4.1	6	0.00767	7.67	1.67
1.3	6	0.00755	7.55	1.55	4.2	6	0.00767	7.67	1.67
1.4	6	0.00760	7.60	1.60	4.3	6	0.00767	7.67	1.67
1.5	6	0.00763	7.63	1.63	4.4	6	0.00767	7.67	1.67
1.6	6	0.00765	7.65	1.65	4.5	6	0.00767	7.67	1.67
1.7	6	0.00766	7.66	1.66	4.6	6	0.00767	7.67	1.67
1.8	6	0.00766	7.66	1.66	4.7	6	0.00766	7.66	1.66
1.9	6	0.00766	7.66	1.66	4.8	6	0.00766	7.66	1.66
2	6	0.00766	7.66	1.66	4.9	6	0.00767	7.67	1.67
2.1	6	0.00766	7.66	1.66	5	6	0.00767	7.67	1.67
2.2	6	0.00766	7.66	1.66	5.1	6	0.00767	7.67	1.67
2.3	6	0.00767	7.67	1.67	5.2	6	0.00766	7.66	1.66
2.4	6	0.00767	7.67	1.67	5.3	6	0.00766	7.66	1.66
2.5	6	0.00767	7.67	1.67	5.4	6	0.00759	7.59	1.59
2.6	6	0.00766	7.66	1.66	5.5	6	0.00755	7.55	1.55
2.7	6	0.00767	7.67	1.67	5.6	6	0.00740	7.40	1.40
2.8	6	0.00767	7.67	1.67	5.7	6	0.00709	7.09	1.09

Figure 21. Values for cladding height

From the obtained chart represented in figure 22 we draw the following conclusion: the first two seconds of processing time have a linear growth from 0 mm, to approximately 1.67 mm. The constant deposition stays from seconds 2 to 5.3 and then a decreasing height occurs from 1.67 mm to 1.09 mm. This downward trend was set because at the end of the program laser optics speed slows down and the accumulation of heat makes the deposition sink into the substrate.

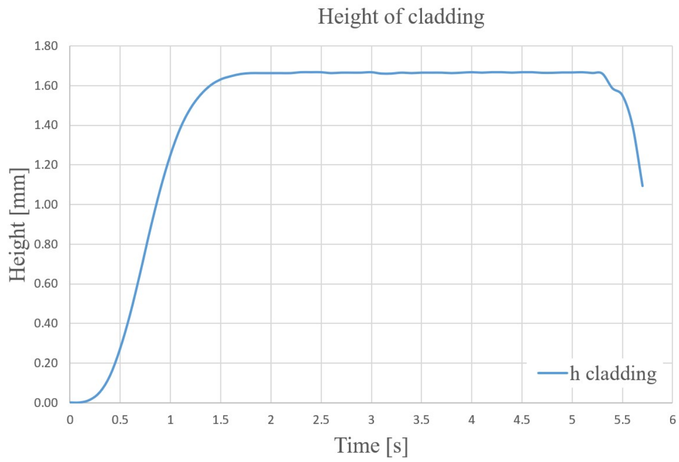

Figure 22. Chart of cladding height

4. CONCLUSIONS

A numerical model combining heat transfer in solids and deformed geometry modules was defined to simulate and predict the temperature field distribution and height of the deposition of metal powder, during cladding process. Using specific parameters for the LMD process and material, the finite element analysis calculates the temperature field and cladding height.

The model can be used only for simulating and predicting temperature distribution and cladding height and has the purpose of reducing the number of experiments and investigations for LMD experiments.

Further research will be focused on comparing the results obtained from computing the numerical program with experiment results, using the same conditions and parameters that we defined in the model.

Another subject that can be developed was enhancing the current model with other physics interfaces like particle tracing for powder particle or computational fluid dynamics for analysis of the melt pool. These modules will increase the veracity of results, but all together will increase the compute time.

5. ACKNOWLEDGEMENTS

We acknowledge the support of National Interest Infrastructure facility IOSIN – CETAL at INFLPR.

6. REFERENCES

1. M. A. Mahmood, D. Chioibasu, S. Mihai, M. Iovea, I. N. Mihailescu, and A. C. Popescu, "Non-Destructive X-ray Characterization of a Novel Joining Method Based on Laser-Melting Deposition for AISI 304 Stainless Steel," *Materials 2021, Vol. 14, Page 7796*, vol. 14, no. 24, p. 7796, Dec. 2021.
2. S. Mihai, F. Baciu, R. Radu, D. Chioibasu, and A. C. Popescu, "In Situ Fabrication of TiC/Ti–Matrix Composites by Laser Directed Energy

Deposition," *Materials 2024, Vol. 17, Page 4284*, vol. 17, no. 17, p. 4284, Aug. 2024.
3. L. Duta *et al.*, "In Vivo Assessment of Bone Enhancement in the Case of 3D-Printed Implants Functionalized with Lithium-Doped Biological-Derived Hydroxyapatite Coatings: A Preliminary Study on Rabbits," *Coatings 2020, Vol. 10, Page 992*, vol. 10, no. 10, p. 992, Oct. 2020.
4. M. Izadi, A. Farzaneh, M. Mohammed, I. Gibson, and B. Rolfe, "A review of laser engineered net shaping (LENS) build and process parameters of metallic parts," *Rapid Prototyp J*, vol. 26, no. 6, pp. 1059–1078, Jun. 2020.
5. S. Mihai, P.-V. Toma, A. Sima, D. Chioibasu, and A. C. Popescu, "A novel method of nondestructive characterization via X-ray and high-speed imaging of TiC/IN718 composite materials manufactured by LMD," *Results in Engineering*, vol. 24, p. 103350, Dec. 2024.
6. D. Chioibasu, S. Mihai, C. M. Cotrut, I. Voiculescu, and A. C. Popescu, "Tribology and corrosion behavior of gray cast iron brake discs coated with Inconel 718 by direct energy deposition," *International Journal of Advanced Manufacturing Technology*, vol. 121, no. 7–8, pp. 5091–5107, Aug. 2022.
7. S. Mihai, D. Chioibasu, M. A. Mahmood, L. Duta, M. Leparoux, and A. C. Popescu, "Real-Time Defects Analyses Using High-Speed Imaging during Aluminum Magnesium Alloy Laser Welding," *Metals 2021, Vol. 11, Page 1877*, vol. 11, no. 11, p. 1877, Nov. 2021.
8. G. Meng, Y. Gong, J. Zhang, L. Zhu, H. Xie, and J. Zhao, "Multi-scale simulation of microstructure evolution during direct laser deposition of Inconel718," *Int J Heat Mass Transf*, vol. 191, p. 122798, Aug. 2022.
9. S. Sarkar, I. V. Singh, and B. K. Mishra, "A simple and efficient implementation of localizing gradient damage method in COMSOL for fracture simulation," *Eng Fract Mech*, vol. 269, p. 108552, Jun. 2022.
10. D. Modupeola and P. Patricia, "Optimizing the maximum strain of a laser-deposited high-entropy alloy using COMSOL multiphysics," *Beni Suef Univ J Basic Appl Sci*, vol. 13, no. 1, pp. 1–8, Dec. 2024.
11. P. Peyre, M. Dal, S. Pouzet, and O. Castelnau, "Simplified numerical model for the laser metal deposition additive manufacturing process," *J Laser Appl*, vol. 29, no. 2, May 2017.
12. F. Caiazzo and V. Alfieri, "Simulation of Laser-assisted Directed Energy Deposition of Aluminum Powder: Prediction of Geometry and Temperature Evolution," *Materials 2019, Vol. 12, Page 2100*, vol. 12, no. 13, p. 2100, Jun. 2019.
13. F. Wirth and K. Wegener, "A physical modeling and predictive simulation of the laser cladding process," *Addit Manuf*, vol. 22, pp. 307–319, Aug. 2018.
14. W. Ya, B. Pathiraj, and S. Liu, "2D modelling of clad geometry and resulting thermal cycles during laser cladding," *J Mater Process Technol*, vol. 230, pp. 217–232, Apr. 2016.
15. B. K. Panda, S. Sarkar, and A. K. Nath, "2D thermal model of laser cladding process of Inconel 718," *Mater Today Proc*, vol. 41, pp. 286–291, 2019.
16. S. Saroj, C. K. Sahoo, and M. Masanta, "Microstructure and mechanical performance of TiC-Inconel825 composite coating deposited on AISI 304 steel by TIG cladding process," *J Mater Process Technol*, vol. 249, pp. 490–501, Nov. 2017, Accessed: Nov. 07, 2024. [Online]. Available: https://www.researchgate.net/publication/317944313_Microstructure_and_mechanical_performance_of_TiC-Inconel825_composite_coating_deposited_on_AISI_304_steel_by_TIG_cladding_process
17. Daniel Ghiculescu, Liviu Nita, Jozsef Pop, and Andrei Rusu, "COMPARATIVE STUDY BETWEEN PLASMA AND LASER CUTTING OF STEELS AND POLYMERIC MATERIALS," in *Revista de Tehnologii Neconventionale*, vol. 26, Nonconventional Technologies Review, 2022, ch. 4, pp. 49–54.
18. J. Ning *et al.*, "Microstructure and mechanical properties of SiC-reinforced Inconel 718 composites fabricated by laser cladding," *Surf Coat Technol*, vol. 463, p. 129514, Jun. 2023.